Auxiliary Material

Magneto-Elastic Coupling in Compressed Fe_7C_3 Supports Carbon in Earth's Inner Core

Bin Chen[1], Lili Gao[2], Barbara Lavina[3], Przemyslaw Dera[4], E. Ercan Alp[2], Jiyong Zhao[2], Jie Li[1]

[1]Department of Earth and Environmental Sciences, University of Michigan, 1100 N. University Ave., Ann Arbor, Michigan 48109, USA.

[2]Advanced Photon Source, Argonne National Laboratory, 9700 S. Cass Ave., Argonne, Illinois 60439, USA.

[3]Department of Physics and Astronomy, University of Nevada, 4505 S. Maryland Pkwy., Box 454002, Las Vegas, Nevada 89154, USA.

[4]Center for Advanced Radiation Sources, University of Chicago, Argonne National Laboratory, 9700 S. Cass Ave., Argonne, Illinois 60439, USA.

Single-crystal X-ray diffraction (XRD)

At Sector 13 of Advance Photon Source (APS), monochromatic X-ray beam with a wavelength of 0.3344 Å was collimated to 5×5 μm^2 at beamline ID-D, and to 15×5 μm^2 at beamline BM-D. X-ray beam with a wavelength of 0.3757 Å was collimated to 15×5 μm^2 at beamline 16-BM-D. In order to collect XRD signals of the sample over a large aperture, we used a cubic boron nitride (cBN) seat on the upstream side and tungsten-carbide seat with 60° opening on the downstream side.

In the first experiment (Run #1), two Fe_7C_3 single crystals, along with ruby spheres as pressure markers [*Mao et al*., 1986], were loaded between one pair of 300 μm-flat diamonds. In the second experiment (Run #2), one Fe_7C_3 single crystal and gold power as pressure markers [*Takemura and Dewaele*, 2008] were loaded between one pair of 100/300-μm beveled diamonds. The setup of the third experiment (Run #3) was similar to Run #1. In all three runs, neon served as pressure medium and the primary pressure marker [*Dewaele et al*., 2008] and was loaded into the DACs using the gas loading system at GeoSoilEnviroCARS (Sector 13) of Advanced Photon Source (APS), Argonne National Laboratory (ANL). At pressures between 19 and 76 GPa in Run #1, the crystals were heated up to 1200 K for stress release, using a double-sided laser system.

The data were processed using the GSE_ADA and RSV software [*Dera et al*., 2008]. Typically 13-34 reflections of Fe_7C_3 were identified and used to extract the lattice parameters (Fig. S1, Fig. S3, and Table S1). The unit-cell volume data of pm- and nm-Fe_7C_3 were fitted using the 3rd-order Birch-Murnaghan (BM) equation of state (EOS),

$$P = \frac{3}{2}K_{0T}\left[\left(\frac{V_0}{V}\right)^{7/3} - \left(\frac{V_0}{V}\right)^{5/3}\right] \times \left\{1 + \frac{3}{4}(K_0' - 4)\left[\left(\frac{V_0}{V}\right)^{2/3} - 1\right]\right\}$$

and Vinet EOS,

$$P = 3K_{0T}\left(\frac{V}{V_0}\right)^{-2/3}\left[1-\left(\frac{V}{V_0}\right)^{1/3}\right]\times\exp\left\{\frac{3}{2}(K_0'-1)\left[1-\left(\frac{V}{V_0}\right)^{1/3}\right]\right\}$$

where K_{0T}, K_0', and V_0 are isothermal bulk modulus, its pressure derivative, and volume at 1 bar, respectively (Table S2).

Synchrotron Mössbauer spectroscopy (SMS)

Two SMS spectra were collected in Run #1, at 66 (±2) GPa and 55 (±1) GPa (on decompression path). SMS measurements at pressures between 1 bar and 8.6 (±0.6) GPa were conducted in Run #2 prior to the XRD measurements. The CONUSS program was used to fit the SMS spectra and extract the magnetic hyperfine parameters [*Sturhahn*, 2004]. We took the calculated local magnetic moments of the three Fe sites from *Fang et al*. [2009] as the initial values to fit the spectrum at ambient condition. After fitting the quadrupole splittings, isomer shifts and site proportions, the local magnetic moments were allowed to change. The procedure was repeated until a good fit was obtained, as indicated by the chi-square value. Above 7 GPa, all the SMS data can be adequately fitted with one Fe site. The hyperfine parameters are listed in Table S3 and plotted in Figure S2.

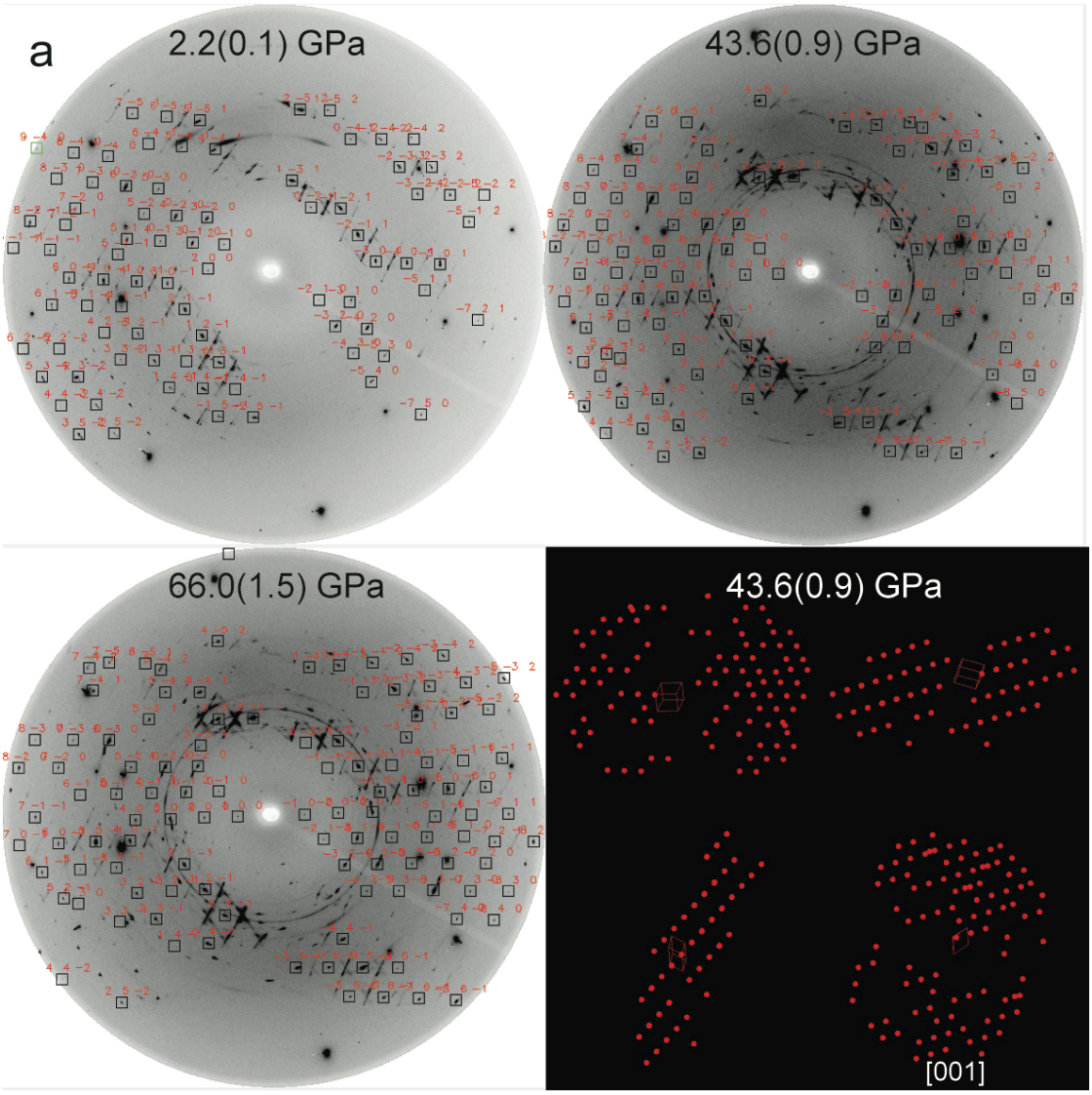
a
2.2(0.1) GPa
43.6(0.9) GPa
66.0(1.5) GPa
43.6(0.9) GPa
[001]

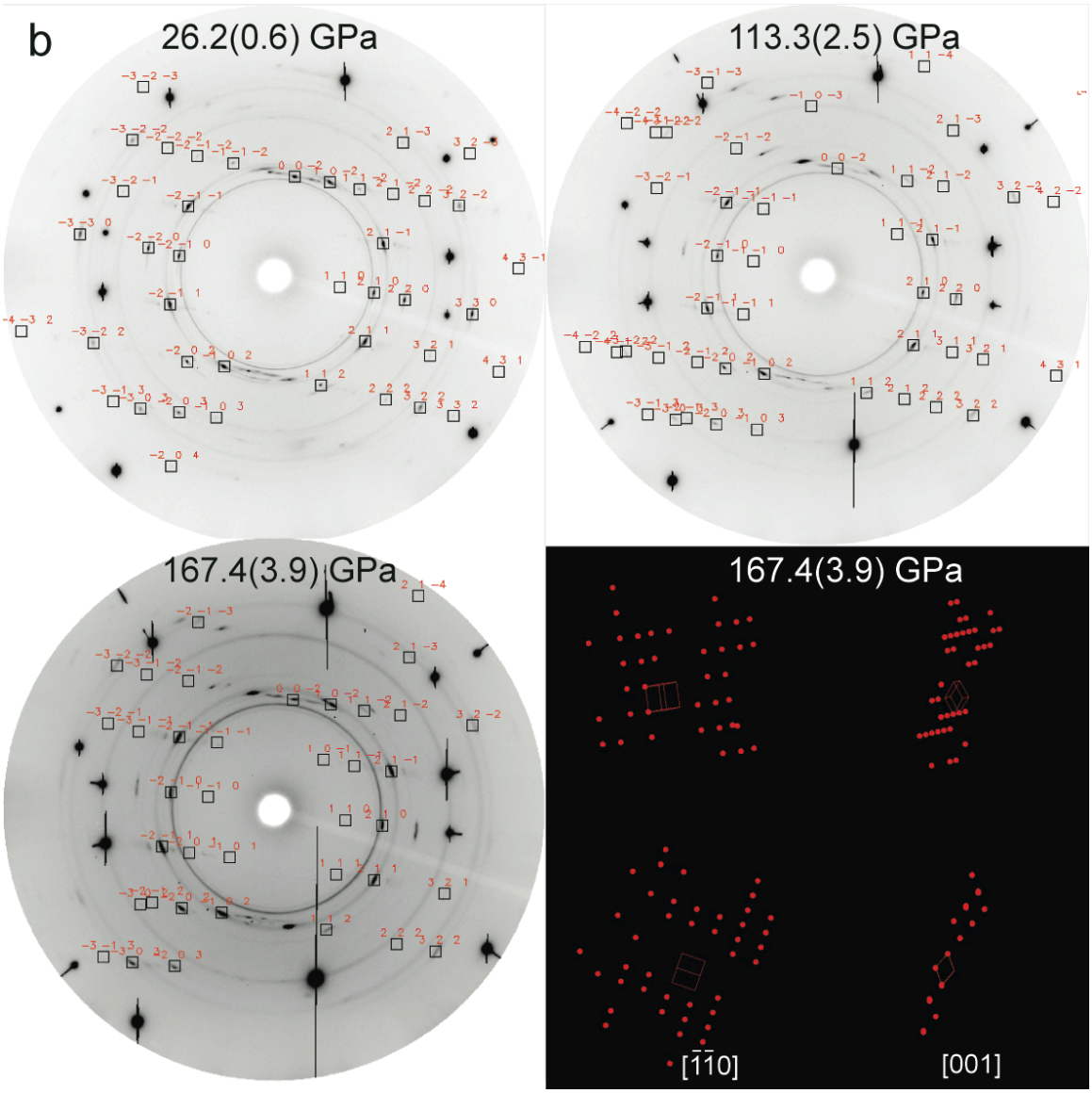

Fig. S1. Representative measured single-crystal X-ray diffraction (XRD) patterns (upper and lower left) and projections of the Fe_7C_3 crystal structure in the reciprocal space along different directions (lower right) in Run #1 (**a**) and Run #2 (**b**). Red labels in the measured patterns correspond to Miller indices (hkl) of the reflections. In the reciprocal space projections, special directions are denoted whereas general directions are not labeled, the top left of which is the projection perpendicular to the X-ray beam.

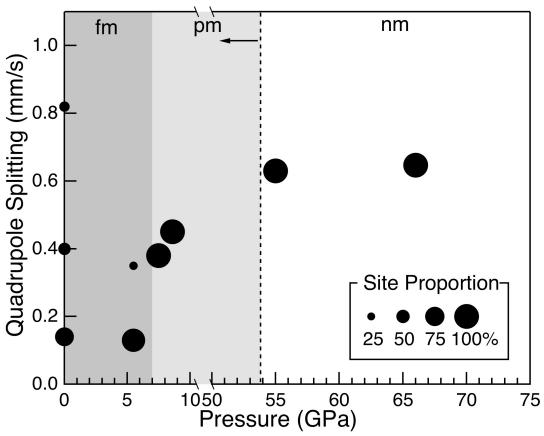

Fig. S2. Quadruple splitting values of various iron sites in Fe_7C_3 as a function of pressure. The sizes of the solid circles correspond to site proportion (Table S3).

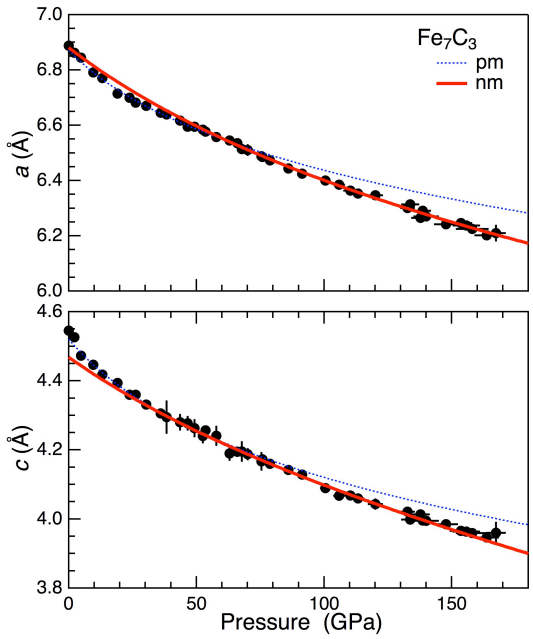

Fig. S3. Lattice parameters *a* and *c* of Fe_7C_3 at 300 K (solid circles) and BM EOS fits to a^3 and c^3 of the pm-phase (blue dotted lines) and nm-phase (red solid lines).

Table S1. Unit-cell parameters and volume of Fe_7C_3 at 300 K.

Run	P_{Ne}[a] (GPa)		V (Å^3)		a (Å)		c (Å)		P_{ruby}[b] (GPa)		P_{Au}[c] (GPa)	
#1	0.0	(0.0)	186.784	(0.706)	6.888	(0.006)	4.545	(0.011)	0.0	(0.0)		
			184.609	(0.336)	6.863	(0.001)	4.526	(0.009)	2.2	(0.0)		
			177.585	(0.361)	6.791	(0.001)	4.447	(0.015)	9.6	(0.0)		
			175.401	(0.561)	6.771	(0.002)	4.418	(0.014)	13.1	(0.6)		
	19.1	(0.6)	171.562	(0.237)	6.715	(0.001)	4.394	(0.006)	20.2	(0.2)		
	23.8	(0.5)	169.472	(0.587)	6.700	(0.002)	4.360	(0.015)	24.0	(0.1)		
	30.4	(0.6)	166.873	(0.430)	6.670	(0.002)	4.331	(0.011)	30.3	(0.3)		
	36.0	(0.7)	164.664	(0.502)	6.645	(0.002)	4.306	(0.013)	35.6	(0.6)		
	43.6	(0.9)	162.267	(0.913)	6.617	(0.002)	4.280	(0.024)	42.3	(0.6)		
	49.2	(1.0)	160.561	(0.985)	6.595	(0.003)	4.263	(0.026)	48.0	(0.5)		
	52.5	(1.6)	159.174	(0.717)	6.584	(0.002)	4.240	(0.021)	50.8	(0.5)		
	57.8	(1.2)	157.895	(0.675)	6.557	(0.003)	4.241	(0.029)	55.3	(0.5)		
	66.0	(1.5)	155.130	(0.633)	6.535	(0.002)	4.195	(0.015)	61.9	(0.5)		
	46.6	(1.2)	161.110	(2.074)	6.595	(0.004)	4.277	(0.021)	45.9	(1.0)		
	38.3	(1.0)	163.939	(1.033)	6.639	(0.003)	4.295	(0.048)	37.9	(1.1)		
	62.9	(1.3)	155.437	(0.597)	6.545	(0.003)	4.190	(0.021)	57.9	(0.6)		
	67.7	(1.4)	154.168	(0.815)	6.514	(0.004)	4.195	(0.030)	70.1	(0.4)		
	75.5	(1.6)	151.895	(0.808)	6.488	(0.003)	4.167	(0.027)	74.0	(0.4)		
#2	26.2	(0.5)	168.564	(0.158)	6.682	(0.003)	4.360	(0.003)			26.4	(0.2)
	53.6	(1.4)	159.448	(0.456)	6.577	(0.010)	4.257	(0.008)			51.2	(0.8)
	70.1	(2.0)	153.718	(0.419)	6.511	(0.021)	4.187	(0.018)			66.8	(0.9)
	75.8	(1.6)	151.997	(0.176)	6.485	(0.003)	4.173	(0.004)			76.4	(0.6)
	78.8	(1.6)	150.933	(0.196)	6.473	(0.004)	4.159	(0.004)			78.2	(0.6)
	86.0	(1.8)	148.946	(0.146)	6.444	(0.003)	4.142	(0.004)			86.6	(0.6)
	91.3	(1.9)	147.572	(0.363)	6.425	(0.009)	4.128	(0.006)			93.2	(0.8)
	100.5	(2.2)	145.059	(0.286)	6.400	(0.007)	4.090	(0.005)			100.6	(0.8)
	105.8	(2.3)	143.611	(0.218)	6.385	(0.006)	4.068	(0.009)			104.1	(0.9)
	110.3	(2.8)	142.659	(0.285)	6.363	(0.007)	4.068	(0.006)			110.8	(1.0)
	113.3	(2.5)	141.888	(0.283)	6.353	(0.007)	4.060	(0.007)			111.7	(1.3)
	120.1	(3.0)	141.034	(0.591)	6.347	(0.012)	4.043	(0.016)			120.1	(1.2)
	133.7	(3.6)	138.034	(0.489)	6.313	(0.014)	3.999	(0.014)			128.6	(1.1)

Run	P_{Ne}[a] (GPa)		V (Å^3)		a (Å)		c (Å)		P_{ruby}[b] (GPa)		P_{Au}[c] (GPa)	
	132.7	(2.9)	138.232	(0.286)	6.301	(0.005)	4.021	(0.007)			131.6	(1.1)
	137.7	(3.7)	136.407	(0.256)	6.265	(0.006)	4.013	(0.008)			135.6	(0.9)
	138.6	(3.3)	136.934	(0.252)	6.291	(0.007)	3.995	(0.007)			138.3	(1.2)
	140.0	(5.0)	136.003	(0.251)	6.270	(0.007)	3.995	(0.008)			140.8	(1.0)
	147.7	(4.7)	134.428	(0.227)	6.241	(0.006)	3.985	(0.006)			147.5	(1.2)
	153.6	(4.4)	134.010	(0.227)	6.246	(0.007)	3.966	(0.007)			154.5	(0.8)
	155.7	(5.4)	133.524	(0.203)	6.237	(0.006)	3.963	(0.005)			155.2	(0.9)
	158.0	(6.5)	132.885	(0.202)	6.225	(0.009)	3.959	(0.005)			158.1	(0.9)
	163.7	(4.8)	131.477	(0.134)	6.202	(0.003)	3.947	(0.003)			165.0	(1.4)
	167.4	(3.9)	132.232	(0.200)	6.210	(0.030)	3.960	(0.032)			162.7	(1.1)
#3	4.8	(0.1)	181.459	(0.167)	6.845	(0.001)	4.472	(0.003)	4.8	(0.1)		

Note: Numbers in parentheses are one standard deviations. Uncertainties in the lattice parameter c in Run #2 are significantly smaller than that in Run #1 because Fe_7C_3 crystal was orientated with [110] direction nearly perpendicular to the diamond culets in Run #2.

[a] Pressure was calculated using the EOS of neon [*Dewaele et al*., 2008].

[b] Pressure was calculated using the Ruby fluorescence calibration [*Mao et al*., 1986]. The compression data using the ruby pressure scale are in good agreements with those using MgO pressure scale from powder XRD measurements by *Nakajima et al*. [2011] up to 71.5 GPa. The pressures from neon pressure scale are generally larger than those from ruby and MgO by 1-3 GPa from 40 to 70 GPa, resulting in a discrepancy between our volume data and those from *Nakajima et al*. [2011] within this pressure range.

[c] Pressure was calculated using the EOS of gold [*Takemura and Dewaele*, 2008].

Table S2. Equation of state parameters of Fe_7C_3.

Phase	V_0 (Å^3)	K_0 (GPa)	K'	EOS type	Notes
pm-Fe_7C_3	184.69(16)	201(12)	8.0(1.4)	BM3	7-53 GPa, this study
pm-Fe_7C_3	184.64(16)	203(11)	7.7 (1.1)	Vinet	7-53 GPa, this study
nm-Fe_7C_3	182.87(38)	307(6)	3.2(1)	BM3	53-167 GPa, this study
nm-Fe_7C_3	182.92(42)	309(8)	3.1(2)	Vinet	53-167 GPa, this study
fm-Fe_7C_3	186.4(1)	201(2)	4.0 (fixed)	BM3	0-18 GPa, *Nakajima et al*. [2011]

BM3: 3rd-order Birch-Murnaghan EOS

Table S3. Magnetic hyperfine parameters of Fe_7C_3.

P (GPa)	Site #	Site Proportion (%)	Quadrupole Splitting (mm/s)	Isomer Shift (mm/s)	Hyperfine Field (T)
0	1	57	0.14(1)	0[a]	15.9(1)
	2	25	0.40(3)	0.006(8)	11.7(1)
	3	18	0.82(2)	0.03(1)	20.6(1)
5.5(1)	1	88	0.13(1)	0[a]	15.4(1)
	2	12	0.35(1)	-0.28(2)	10.6(1)
7.5(3)	1	100	0.38(1)	-	0
8.6(6)	1	100	0.45(1)	-	0
55 (1)	1	100	0.63(1)	-	0
66 (2)	1	100	0.65(1)	-	0

Numbers in parentheses indicate the uncertainties in the last digit.

[a] The isomer shift is fixed to zero for this site.

References

Dera, P., B. Lavina, L. A. Borkowski, V. B. Prakapenka, S. R. Sutton, M. L. Rivers, R. T. Downs, N. Z. Boctor, and C. T. Prewitt (2008), High-pressure polymorphism of Fe_2P and its implications for meteorites and Earth's core, *Geophys. Res. Lett.*, *35*, L10301, doi:10.1029/2008GL033867.

Dewaele, A., F. Datchi, P. Loubeyre, and M. Mezouar (2008), High pressure--high temperature equations of state of neon and diamond, *Phys. Rev. B*, *77*(9), 094106.

Fang, C. M., M. A. van Huis, and H. W. Zandbergen (2009), Structural, electronic, and magnetic properties of iron carbide Fe_7C_3 phases from first-principles theory, *Phys. Rev. B*, *80*, 224108+, doi:10.1103/PhysRevB.80.224108.

Mao, H. K., J. Xu, and P. M. Bell (1986), Calibration of the ruby pressure gauge to 800 kbar under quasi-hydrostatic conditions, *J. Geophys. Res.*, *91*(85), 4673–4676.

Nakajima, Y., E. Takahashi, N. Sata, Y. Nishihara, K. Hirose, K. Funakoshi, and Y. Ohishi (2011), Thermoelastic property and high-pressure stability of Fe_7C_3: Implication for iron-carbide in the Earth's core, *Am. Mineral.*, *96*(7), 1158–1165, doi:10.2138/am.2011.3703.

Sturhahn, W. (2004), Nuclear resonant spectroscopy, *J. Phys. Condens. Matter*, *16*(5), 497–530.

Takemura, K., and A. Dewaele (2008), Isothermal equation of state for gold with a He-pressure medium, *Phys. Rev. B*, *78*(10), 104119.